



ISSN: 0067-2904

Computer Vision of Optimal Geometric Concentration Ratio for the Solar Ball Lens

Sabah M. Hadi*¹, Manal M. Abdullah¹, Mohamed S. Mahdi²

¹Department of Physics, College of Science, University of Baghdad, Baghdad, Iraq

²Department of solar energy, renewable energy directorate, Ministry of science and technology, Baghdad, Iraq

Received: 19/9/2021

Accepted: 24/1/2022

Published: 30/9/2022

Abstract:

This research evaluates the optical properties of an inhomogeneous and non-paraxial system using a solar ball lens (SBL) as a new thermal solar concentrated collector. This evaluation is based on detecting a diacaustic curve in a straightforward and accurate manner, with the diagnostic relying on image processing as a computational tool using the MATLAB program rather than a complicated numerical analytic procedure. The circle of least confusion (CLC) of the (SBL), (Fluorinated ethylene propylene (FEP) polymer – water core), was calculated. Furthermore, the study evaluated the maximum geometrical concentration ratio (G C) of refracted solar radiation that can be captured by a receiver of the (SBL). Without energy losses due to spherical aberration, the (G C) ratio was (14.10) at (h/r) ratio, circular aperture radius to ball radius, around (0.6). The investigation also revealed an aplanatic point for preventing the development of optical envelope inside the solar ball lens at (h/r) equal to 0.8638, as well as a maximum (h/r) value of 0.7351 for collecting solar radiation.

Keywords: solar ball lens, image processing, diacaustic curve, circle of least confusion (CLC).

رؤية الحاسوب لنسبة التركيز الهندسي الأمثل لعدسة الكرة الشمسية

صباح محمد هادي^{1*}, منال مدحت عبدالله¹, محمد صالح مهدي²

¹قسم الفيزياء، كلية العلوم، جامعة بغداد، العراق

²قسم الطاقة الشمسية، دائرة الطاقات المتجددة، وزارة العلوم والتكنولوجيا، بغداد، العراق

الخلاصة

الهدف من البحث هو تقييم الخصائص البصرية لنظام غير متجانس وغير محوري باستخدام عدسة كروية شمسية (SBL) كمجمع حراري شمسي جديد. يعتمد هذا التقييم على تشخيص منحنى (diacaustic) بطريقة مباشرة ودقيقة، باعتماد التشخيص على المعالجة الصورية كأداة حسابية باستخدام برنامج MATLAB بدلاً من إجراء تحليلي رقمي معقد. تم حساب دائرة التشنت الأقل (CLC) لـ (SBL)، غلاف كروي من بوليمر (FEP, Fluorinated ethylene propylene) وماء. قيمت الدراسة الحد الأقصى لنسبة التركيز الهندسي (GC) للإشعاع الشمسي المنكسر الذي يمكن التقاطه بواسطة مستقبل (SBL)، وبدون فقد الطاقة بسبب الزيغ الكروي، فكانت نسبة التركيز الهندسي (14.10) عند (r / h) والتي تمثل نسبة نصف قطر

*Email: sabahhadi725@gmail.com

الفتحة الدائرية إلى نصف قطر الكرة ، هي (0.6). ومن خلال هذه الدراسة تم تحديد نقطة a. (aplanatic) لمنع تكون الغلاف البصري داخل العدسة الكروية الشمسية عند (h / r) يساوي 0.8638، بالإضافة الى ذلك تم تحديد نسبة (h / r) التي يكون عندها أعلى قيمة لتجميع الإشعاع الشمسي والتي تساوي (0.7351) .

1. Introduction:

The world is working to ensure that clean, limitless energy resources are produced [1]. So, the solution is to enhance energy generation from renewable energy resources, which are abundant and environmentally friendly [2,3]. Solar energy is widely acknowledged as a vital and easily obtainable energy source among renewable alternatives [3-5]. In general, photovoltaic modules are used to directly generate electrical energy in solar energy systems and direct heat generation from thermal solar collectors. In addition, hybrid systems generate both direct electrical energy and indirect thermal energy [6]. Concentrated solar power (CSP) technique may cover both thermal and electrical requirements. In (CSP) technology, mirrors or lenses focus sun beams on a specific targeted spot (CSP). Technologies in use now include the parabolic trough collector (PTC), solar power tower (SPT), parabolic dish systems, and linear Fresnel reflector (LFR). Figure 1 shows a typical solar concentrator [7].

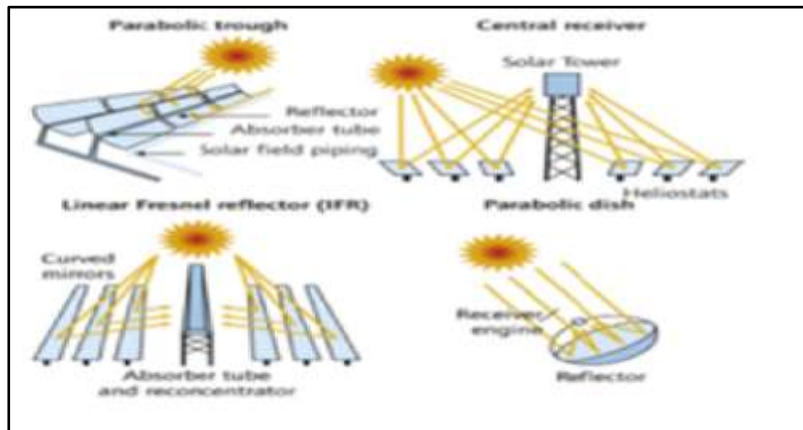


Figure 1- A typical solar concentrator [7]

These varieties of (CPS) concentrators must be oriented in the direction of the sun in the sky. As a result, the system necessitates bulkier movement and heavy-duty motors with higher electrical energy consumption [8]. Andre Broessel created a spherical sun-tracking solar energy generator to generate sustainable energy while minimizing the use of tracking energy. Figure 2 shows a sketch of Andre Broessel invention [9].

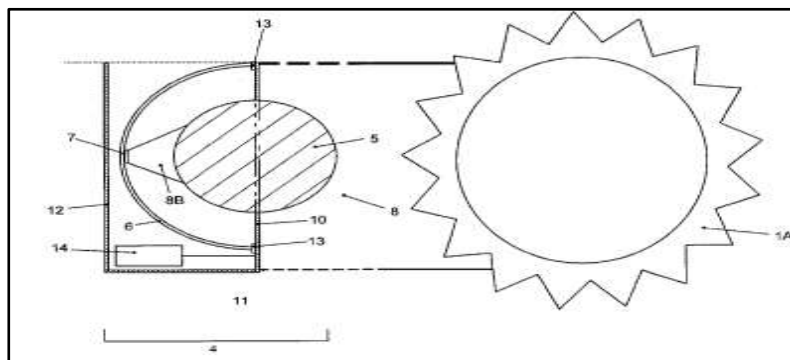


Figure 2-A sketch for the invention related to an energy concentrator system for directly converting solar energy into thermal energy [9].

Later, Rawlemon improved the Andre Broessel design by combining a spherical lens to focus light on a small photovoltaic panel with a dual-axis pivot that tracks the movement of the sun. Solar collecting capabilities are 35% more efficient than the traditional dual-axis photovoltaic designs. Figure 3 illustrates the structure and operation of Rawlemon solar ball lens [10].



Figure 3- This figure illustrates (a) Structure of solar ball lens, (b) solar ball lens working principal [10].

The contribution in this study was made by evaluating the Circle of Least Confusion (C.L.C.) of a solar ball lens in a practical method, using digital image processing. This technique was used to reveal the diacaustic curve equation instead of the difficulties of the numerical analysis method. Furthermore, the equation of the marginal ray was obtained using the ray tracing method as a necessary condition for determining (C.L.C.) and geometrical concentration (G.C.).

2.Theory:

Under paraxial approximation, a spherical ball lens was given two equations: an effective focal length (EFL) and a back focal length (BFL) equations, Equations (1) and (2), respectively. Figure (4-a) shows the geometrical shape of a homogeneous spherical ball lens in paraxial approximation [11]:

$$EFL = \frac{n r}{2(n - 1)} \tag{1}$$

$$BFL = EFL - r \tag{2}$$

Where: n is the refractive index of the sphere and (r) is the radius of the sphere. The EFL is a measure from the center of the ball lens, and the BFL from its rear surface.

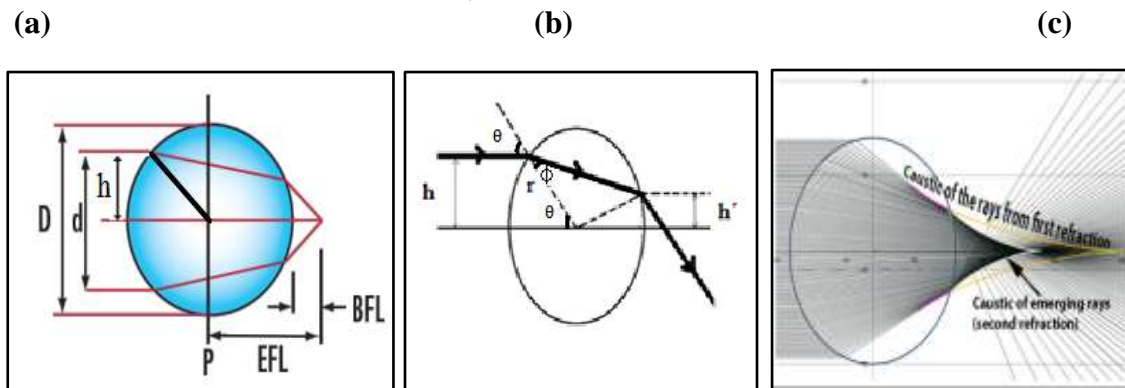


Figure 4- (a) The geometrical parameters of a homogeneous spherical ball lens in paraxial approximation [11], (b) sketch of a converging sphere lens, (c) the two caustic curves of the refracted rays given by the first refraction and second refraction in non-paraxial case [12].

A Non-paraxial case is when a light ray interacts with either a reflective surface or refractive surface, it bends and changes its path. The caustic surface is an optical envelope generated by the refracted rays. In a ball lens, there are two caustic refractive surfaces: the

first, internal caustic generated by the first refraction and the outer caustic surface (diacaustic) formed by the second refraction (emerging rays). Figure (4-c) demonstrates the two caustic curves of the refracted rays created by the first and second refraction in a non-paraxial case [12]. A caustic curve inside a homogeneous ball lens is caused by refracted parallel incident rays inside homogeneous ball lens is discussed in different mathematics methods, the ray tracing method which depends on triangular functions is one of them [Equation (3)]:

$$x_{caustic} = - \frac{r \left[\cos\phi \cdot \cos(\phi - \theta) + \cos\phi \left(\frac{d\phi}{d\theta} - 1 \right) \right]}{\left(\frac{d\phi}{d\theta} - 1 \right)} \tag{3}$$

Where: θ , ϕ , and x are incident angle, refractive angle, caustic coordinate, respectively. Another ray tracing method depending on curvilinear coordinate was applied by Burkhard and Shealy to evaluate caustic curve formed by parallel incident rays on refracted spherical surface as a result of their research. The study explains the unit vector (A) in the direction of refracted ray when incident ray is at the negative z-direction, as illustrated in Equations (4), and (5) [13]:

$$a = -\alpha i - \beta j - \gamma k \tag{4}$$

$$A = \left\{ \left[\gamma \sin\theta \cos\theta \cos\phi - \sin\theta \cos\phi (1 - \gamma^2 \sin^2\theta)^{\frac{1}{2}} \right] i + \left[\gamma \sin\theta \cos\theta \sin\phi - \sin\theta \sin\phi (1 - \gamma^2 \sin^2\theta)^{\frac{1}{2}} \right] j \right. \\ \left. + \left[-\gamma \sin^2\theta - \cos\theta (1 - \gamma^2 \sin^2\theta)^{\frac{1}{2}} \right] k \right\} \tag{5}$$

Furthermore, cusp catastrophe explains the caustic surface; when light propagates through an imperfect focusing system, a cusp catastrophe occurs, in which caustics is a manifestation of catastrophe theory in optics [11]. The intensity of a point caustic is described by the Airy function, and the phase takes the shape of a fold catastrophe, as in Equation (6) [14].

$$Ai(z) = \frac{1}{2\pi} \int_0^{\infty} e^{i\left(zx + \frac{x^3}{3}\right)} dx \tag{6}$$

The Airy function, in its general case, is the Pearcey function, except instead of being in one dimension, z, it is in two dimensions, z and y. Equation (7) shows Pearcey function [15]:

$$p(z, y) = \int_{-\infty}^{\infty} e^{i\left(\frac{zt+yt^2}{2+t^4}\right)} dt \tag{7}$$

Zeeman Catastrophe Machine describes the cusp catastrophe (caustic corresponds to the optical phenomenon) by Fourth polynomial degree as a truncated form as in Equation (8):

$$(\theta) \approx a_0 + a_1\beta\theta + a_2\alpha\theta^2 + a_3\beta\theta^3 + \theta^4 \tag{8}$$

Coordinates domain movement are α , β , and the potential energy of this system is a function of angle θ , the standard form of the cusp catastrophe find as a control parameter given by Equation(9)

$$v(q) = aq + \frac{1}{2}bq^2 + \frac{1}{4}q^4 \tag{9}$$

Where: a, b are control parameters that can be represented by shifting the origin of θ to $q = \theta + a_3\beta/4a_4$ [16].

The shelled ball lens was researched by Elagha [17]who explained the focus distance when a parallel incident ray passes through a shelled ball lens, as in Equation (10):

$$\frac{1}{B} = \frac{1}{h} \sin \left[2 \sum_{i=1}^N \left(\sin^{-1} \frac{h}{r_i \prod_{p=1}^i \mu_{p-1}} - \sin^{-1} \frac{h}{r_i \prod_{p=1}^i \mu_p} \right) - \theta \right] \tag{10}$$

Where: B is the focus distance, N is the number of shells, r_i is the radius of the i^{th} shell encountered when travelling out from the center of the lens, and μ_p is the relative refractive index at the p^{th} surface encountered when travelling out from the center of the lens, i.e., $\mu_p = \mu_p / \mu_p - 1$. A solar ball lens is a hollow shell filled with water; this solar ball lens with two surfaces of spherical shell was evaluated for parallel incoming ray at height (h) and $\theta = 0$ as in Equation (11) [17]

$$\frac{1}{B} = \frac{1}{h} \sin \left[2 \left(\sin^{-1} \frac{h}{r_1} - \sin^{-1} \frac{h}{r_1 \mu_1} + \sin^{-1} \frac{h}{r_2 \mu_1} - \sin^{-1} \frac{h}{r_2 \mu_2 \mu_1} \right) \right] \quad (11)$$

3. Result and discussion

3.1 Relation optical envelop with radius of rear spot

Ray tracing method was applied on solar ball lens (SBL) in assistant of MATLAB program. Polymer (FEP) was chosen as shells with refractive index (1.344) for 630nm wavelength. The ray tracing method is shown by the (h / r) ratio versus (h / h') ratio for the FEP polymer at various thickness-to-ball radius ratios (t/r) (0.001, 0.05, and 0.1), as in Figure 5-c. Figure 5-a shows a photo of shelled ball (FEP– pure water) irradiated by solar radiation with its sketch in Figure 5-b.

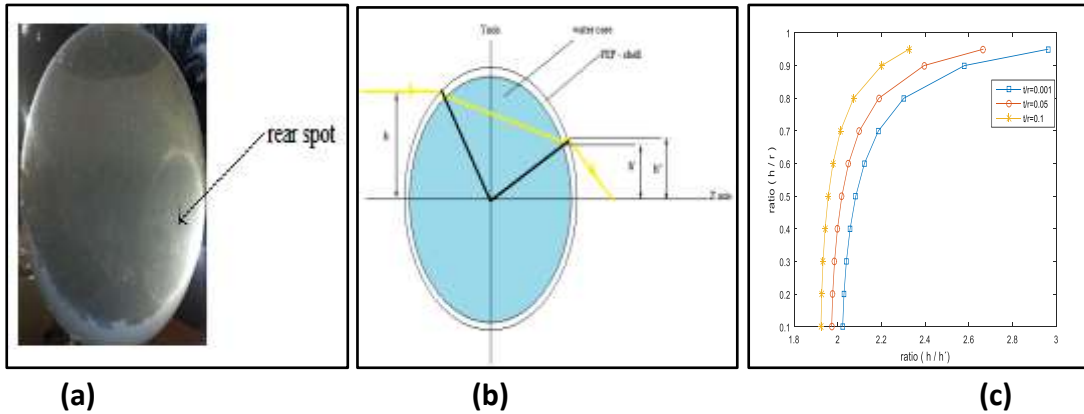


Figure 5-(a) a photo of shelled ball (FEP– pure water) irradiated by solar radiation, (b) sketch of solar ball lens, and (c) (h / r) ratio vs. (h / h') ratio for polymer FEP.

Figure 5-c shows that the (h / h') ratio rises gradually until the ratio (h / r) exceeds 0.8, at which point the (h / h') ratio rises dramatically. Furthermore, an increase in the (t/r) ratio value resulted in an increase in the (h / h') value. An aplanatic point should be determined to prevent spherical aberration (in optical spherical surfaces). A roughly aplanatic point is calculated as a function of the sphere's radius to the lens material's refractive index. Accordingly, the radius of the sphere (r) is a function of the aplanatic point. An accurate value of the aplanatic point of the inhomogeneous lens was theoretically obtained using a specific sphere with radius (r) = 12.5255cm and shell thickness (t) = 1.5mm.

Figure 6 illustrates the relation between the change of aperture radius of the lens (h) and its back rear spot radius h'. A non-linear relation is clearly noticed as the aplanatic point is reached, which is the deflection point of the curve. So, the aplanatic points of inhomogeneous lenses made of one of the polymer shells (FEP) with a shell thickness of 1.5 mm is (h/r) = 0.8638. The graphical relationship curve revealed that the relation has two behaviors; the first is an increase in h' value up to the aplanatic point, and the second is a decrease in h' value when (h/r) value is exceeded. The result can be attributed to spherical aberration inside the lens caused by the intersection of rays inside the non-homogeneous lens and refracted rays at different angles; the intersection rays caused a large spherical aberration above the aplanatic point. These rays that intersected each other created optical envelopes, which optically are known as a ray family that built the caustic curve. In addition, the low spherical aberration is caused by refracted rays at different angles without intersections.

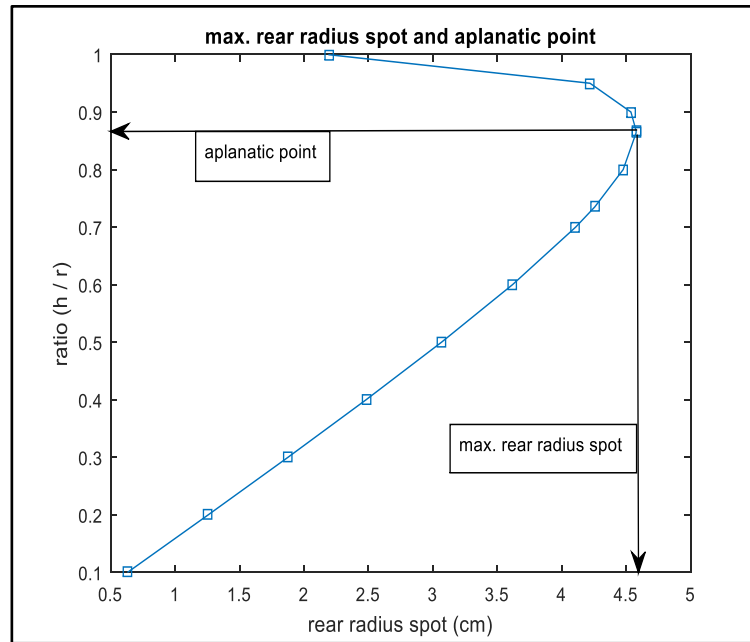


Figure 6-The maximum radius rear spot of aplanatic point of the inhomogeneous (polymer (FEP) shell -water core) sphere with shell thickness= 1.5 mm. The wavelength = 630nm. The arrow represents the aplanatic point at (y) axis. h" at (x) axis.

3.2 Circle of least confusion (C.L.C.).

It is commonly known that there is a plane in which the focused bundle of rays has the smallest diameter; this plane is described as having the best geometrical focus. If the margin ray from lower portion of the lens is considered, the (CLC) is located at the intersection of a margin ray and the caustic curve of the incident ray from the upper part [18]. The caustic equation from a spherical surface of a homogenous optical material and the source off-axis is analytically complicated [19]. Analytically, determining the caustic curve is difficult because it requires solving an equation of the 12th degree employing numerical analysis methods. [20]. The diacaustic equation curve will be more complicated in the system of (SBL), a non-homogeneous optical material (shell and core) with off-axis (converged rays) at the rear of (SBL). Thereby, as a result, image processing was used in this study to help in the evaluation of the solar diacaustic curve equation as a major requirement for determining (CLC).

3.2.1 – Determination of diacaustic curve equation.

The diacaustic curve equation of the (SBL) was investigated in the same specifications as the computerized evaluation in section 3.1. The intensity distributions of the focal spot on the (y-z) plane of the solar ball lens irradiated by solar radiation were captured (Figure 7-a). The captured image properties are JPEG image dimensions(3264x2448), f-stop of the lens f/2, and 4mm focal length. The field of view (FOV), working distance (WD), and sensor size (H) were used to determine the actual size of the pixel represented in the image, which was 0.0044cm. The edge detection was applied using canny order with a suitable threshold to avoid losing image information(Figure 7-b). The diacaustic curve was then revealed using additional treatments in the MATLAB program, which was employed as an image processing tool (Figure 7-c).

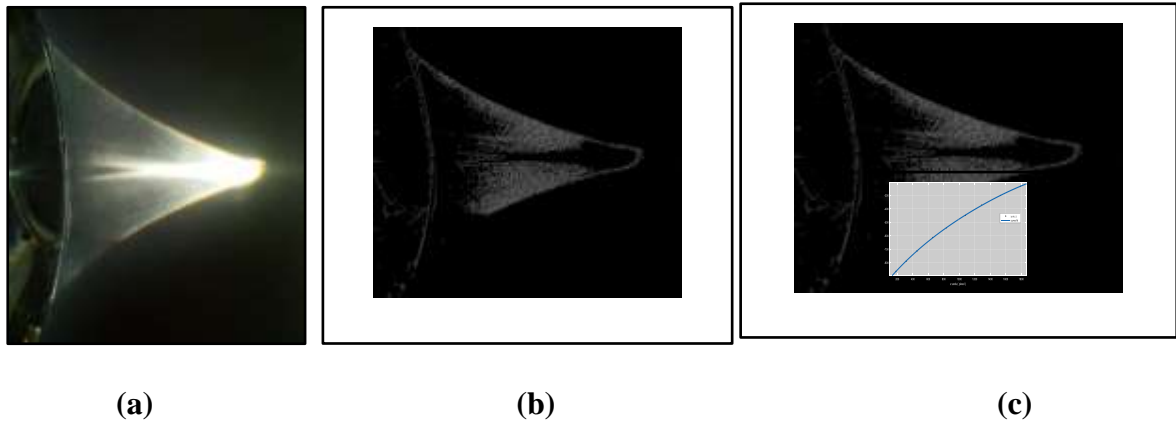


Figure 7-The focused pattern of solar ball lens (a) captured image in (y-z) plane, (b) edge detection canny order, and (c) extracted caustic curve equation.

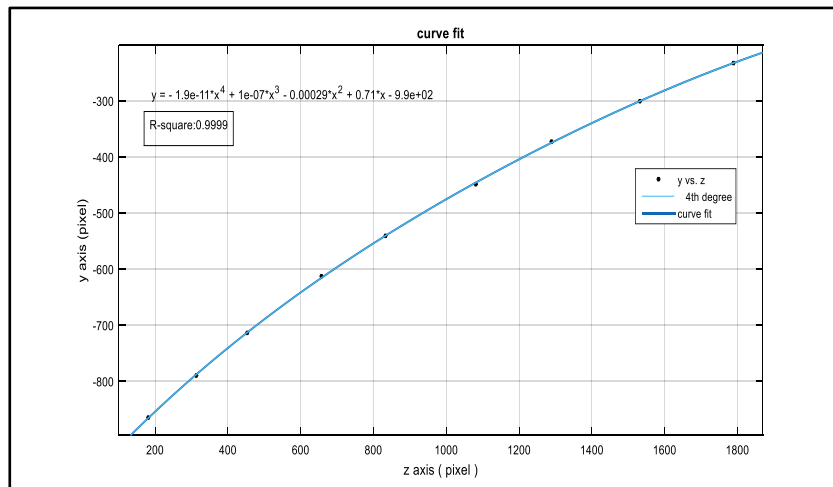


Figure 8- Demonstration of the diacaustic curve fitting.

The curve fitting (R-square 0.9999) revealed 4th degree polynomial equation of lower curve diacaustic in the (y-z) plane, which represents unstandardized cusp catastrophe equation, Equation (12), without adopting control parameters as mentioned in Equation (8).

$$y = -1.916 \times 10^{-11} z^4 + 1.03 \times 10^{-7} z^3 - 0.0002857 z^2 + 0.7123 z - 986.2 \quad (12)$$

3.2.2 Determine equation of marginal ray.

The upper marginal ray equations that intersect with the lower diacaustic curve was found by three steps. The first step, uses the ray tracing method to determinate the emerging points on the rear of the solar ball lens, h" points (z, y) as shown in Figure 8. The second step represents finding the EFL coordinate points of the shelled ball lens which is extracted by Equation (11). These points, together with their corresponding (h/r) ratios, are listed in Table 1.

Table 1- Emerging rays coordinate points.

h/r	h (cm)	EFL point (y, z)	h" point(y, z)
0.1	1.2525	(0, 24.3291)	(0.6297, 12.5097)
0.2	2.5051	(0, 24.0476)	(1.2560, 12.4624)
0.3	3.7577	(0, 23.5676)	(1.8750, 12.3844)
0.4	5.0102	(0, 22.8688)	(2.4812, 12.2773)
0.5	6.2628	(0, 21.9105)	(3.0667, 12.1443)
0.6	7.5153	(0, 20.5889)	(3.6177, 11.9917)
0.7	8.7679	(0, 18.2916)	(4.1079, 11.8327)
0.7351	9.2079	(0, 13.2412)	(4.2563, 11.7801)

The computer functions two points of the emerging marginal ray: (h" point (y, z) and EFL point (y, z)), Equation (13) represents the equation of the marginal ray as the third step. This equation is determined with R- square: 1, (optimal case of curve fitting). the coefficients values of (p₁ and p₂) are listed in Table 2.

In addition, the highest (h/r) ratio contributing to the focal spot was (0.7351). As a result, above this ratio value no effect on the focus spot in the (y, z) plane was noticed.

$$y = p_1 \cdot z + p_2 \tag{13}$$

Table 2- Emerging ray liner equation coefficients

h/r	P ₁	P ₂
0.1	-0.05328	1.296
0.2	-0.1084	2.607
0.3	-0.1677	3.951
0.4	-0.2343	5.357
0.5	-0.314	6.88
0.6	-0.4208	8.664
0.7	-0.636	11.63
0.7351	-2.913	38.57

In a solar ball lens, the geometrical concentration ratio is calculated by dividing the aperture area by the circle of least confusion (CLC), which represents the geometrically best focus plane. The two intersection points coordinates of the upper emerging marginal rays with the lower diacaustic curve and vice versa determine the diameter of CLC. The circular (CLC) area and geometrical concentration ratio (G.C) with respect to the (h / r) ratio are shown in Table 3.

Table 3- plane of (CLC) and (G.C)

h/r	h (cm)	CLC (cm ²)	G.C
0.1	1.2525	1.059	4.65
0.2	2.5051	2.614	7.54
0.3	3.7577	4.596	9.65
0.4	5.0102	6.847	11.52
0.5	6.2628	9.421	13.08
0.6	7.5153	12.582	14.10
0.7	8.7679	17.974	13.44
0.7351	9.2079	42.983	6.19

As a result, with aperture (h/r) = 0.6, the (SBL) can achieve its maximum concentration ratio. This aperture corresponds to the (G.C) of 14.1 which is the geometrical ratio of maximum collecting solar radiation without loss of solar energy due to spherical aberration, as shown graphically in Figure-9.

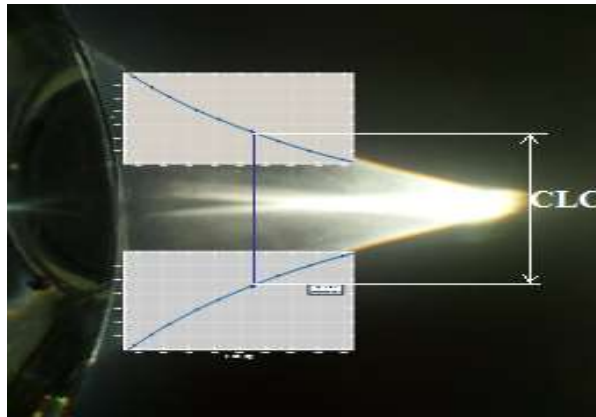


Figure 9- The (CLC) plane with maximum geometrical concentration without losses of solar energy by spherical aberration.

4. Conclusions:

The solar ball lens was successfully evaluated; the evaluation depends on image processing as a computational tool employing the MATLAB program, rather than a complicated numerical analytic method, to determine a diacaustic curve in a direct and accurate method. Through this study, graphical relationships were found that link many interesting variables, through which it was possible to find optimal receiver size dimensions. The analysis results of the experimental solar ball lens revealed that the geometrical concentration ratio ranged from (4.65) to (14.10) for (h/r) ratio (ball lens aperture radius to its radius) from (0.1) ratio to (0.7351) the highest possible ratio could be advantageous.

References

- [1] A. Messai, Y. Benkedda, S. Bouaichaoui and M. Benzerga, "Feasibility study of parabolic trough solar power plant under," in *The Mediterranean Green Energy Forum, MGEF-13*, Fes, Morocco, 2013.
- [2] S. M. Khazael and M. Al-Bakri, "The Optimum Site Selection for Solar Energy Farms using AHP in GIS," *Iraqi Journal of Science*, vol. 62, no. 11, pp. 4571-4587, 2021.
- [3] E. K. Mpodi, Z. Tjiparuro and O. Matsebe, "Review of dual axis solar tracking and development," in *2nd International Conference on Sustainable Materials Processing and Manufacturing*, Sun City, South Africa, 2019.
- [4] M. B. Al-hadith and Y. M. Tayib, "Design and Performance Analysis of Spiral Solar Water Heater Using Iron," *Iraqi Journal of Science*, vol. 62, no. 11, pp. 4290-4299, 2021.
- [5] M. T. Islam, N. Huda, A. B. Abdullah and R. Saidur, "A comprehensive review of state-of-the-art concentrating solar power (CSP)," *Renewable and Sustainable Energy Reviews*, vol. 91, pp. 987-1018, 2018.
- [6] S. Seme, B. Štumberger, . M. Hadžiselimovi'c and K. Sredenšek, "Solar Photovoltaic Tracking Systems for Electricity," *Energies*, vol. 13, no. 16, p. 4224, 2020.
- [7] W. Fuqiang, . C. Ziming, T. Ziming, Y. Yuan, . S. Yong and . L. Linhua, "Progress in concentrated solar power technology with parabolic trough," *Renewable and Sustainable Energy Reviews*, vol. 79, pp. 1314-1328, 2017.
- [8] C. Goel and S. Yoo, "Hybrid daylight harvesting system using static ball lens concentrator and," *Solar Energy*, vol. 2016, pp. 121-132, 2021.
- [9] B. A and P. M, "Energy convertor/concentrator system". U.S.A. Patent 13/984,323, 26 Jun 2014.
- [10] H. ABDULMOUTI, M. A. ALMARZOOQI, A. A. ALMULLA, M. J. KHAIR, H. H. ALYASI, A. A. ALJASMI and Y. M. ALMULLA, "Generating Power from Solar Sphere Design," in *Advances in Science and Engineering Technology International Conferences (ASET)*, Dubai, United Arab Emirates, 2019.

- [11] M. S. Kim, T. Scharf, S. Mühlig, M. Fruhnert, C. Rockstuhl, R. Bitterli, W. Noell, R. Voelkel and H. P. Herzig, "Refraction limit of miniaturized optical systems:," *Optical Society of America*, vol. 24, no. 7, pp. 6996-7005, 2016.
- [12] P. Mihas, "Excel Files for Teaching Caustics of Rainbow and Lenses," *Journal of Physics & Optics*, vol. 3, no. 1, pp. 2-7, 2021.
- [13] D. G. Burkhard and D. L. Shealy, "Flux density for ray propagation in geometrical optics," *JOURNAL OF THE OPTICAL SOCIETY OF AMERICA*, vol. 63, no. 3, pp. 299-304, 1973.
- [14] J. H. J. B and S. B, *Methods of mathematical physics*, Cambridge: Cambridge university press, 1999.
- [15] J. J. Stamnes and B. Spjelkavik, "Evaluation of the field near a cusp of a caustic," *Optica Acta: International Journal of Optics*, vol. 30, no. 9, pp. 1331-1358, 1983.
- [16] D.A.MacBeath, "The Pearcey function and the cusp catastrophe," M.Sc.dissertation, Dept. Phy. sci., McMaster University, Hamilton, Ontario, 2016.
- [17] E. . H. A, "Ray tracing in monocentric and ball lenses by a general exact formula," *JOSA A*, vol. 36, no. 7, pp. 1117-1125, 2019.
- [18] R. W. Hosken, "Circle of least confusion of a spherical reflector," *Applied optics*, vol. 46, no. 16, pp. 3107-3117, 2007.
- [19] D. G. Burkhard and D. L. Shealy, "Formula for the density of tangent rays over a caustic surface," *Applied Optics*, vol. 21, no. 18, pp. 3299-3306, 1982.
- [20] M. Avendaño-Alejo, L. Castañeda and I. Moreno, "Properties of caustics produced by a positive lens: meridional rays," *JOSA A*, vol. 27, no. 10, pp. 2252-2260, 2010.